Supplementary File

Historical and Projected Changes in Temperature–Precipitation Compound Hot and Dry Extremes across Africa Based on CMIP5 and CMIP6 Ensemble Simulations

Paul Adigun [1]; Koji Dairaku [1]; Akinwale T. Ogunrinde [2,*]; Ebiendele Precious [1]; Muhammad Umar Nadeem [1]; Ermias Sisay Brhane [1]; Xian Xue [1]

[1] *Department of Engineering Mechanics and Energy, University of Tsukuba, 3F300 Tennodai 1-1-1, Tsukuba, 305-8573, Japan.*

[2] *Key Laboratory of Ecological Safety and Sustainable Development in Arid Lands, Northwest Institute of Eco-Environment and Resources, Chinese Academy of Sciences, Lanzhou, Gansu, China*

* Corresponding author: ogunrindeakinwale@nieer.ac.cn

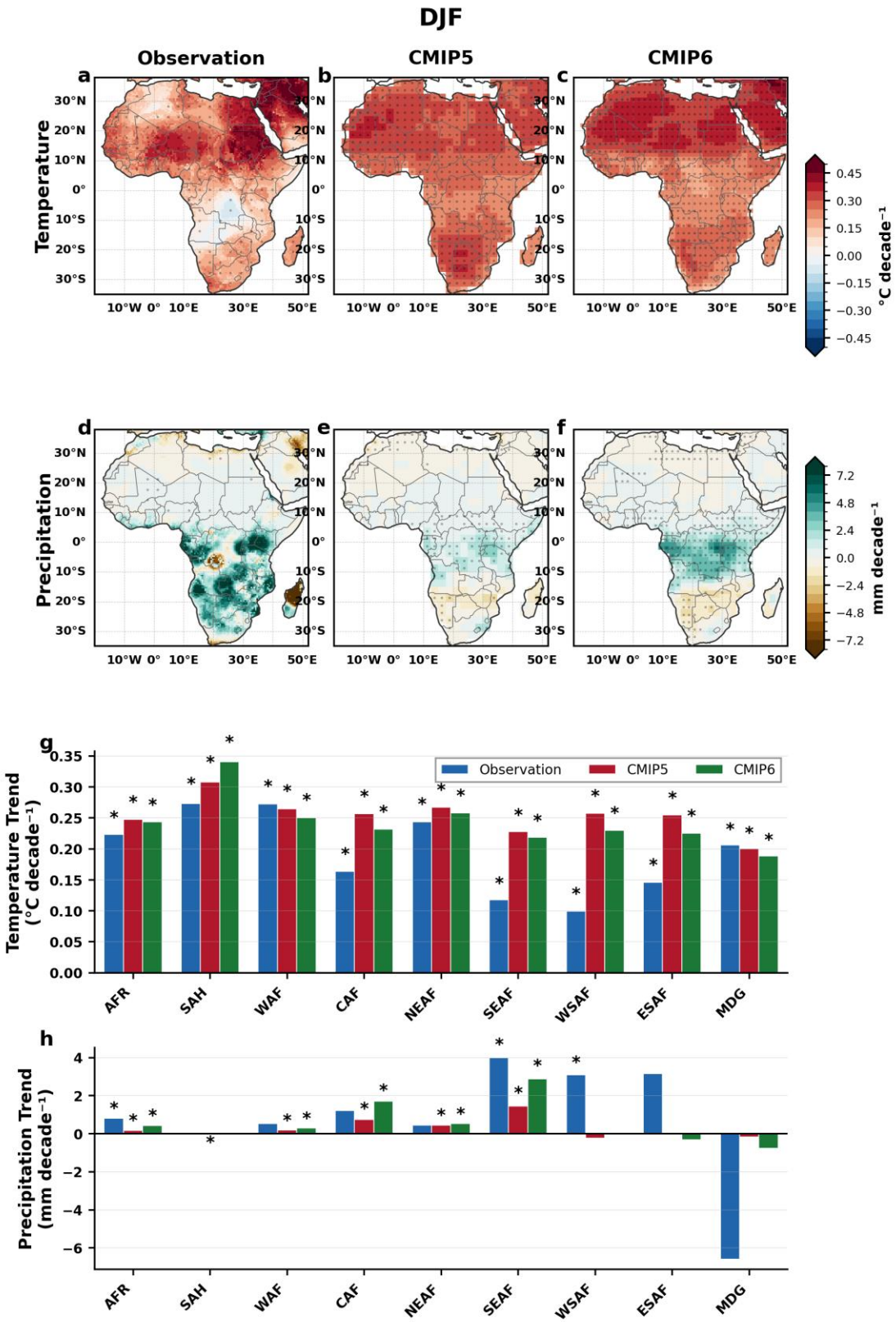

Figure S1: Seasonal temperature and precipitation trends for DJF (December–January–February), 1980–2020. Layout as in Fig. 1. DJF represents the boreal winter and austral summer season. Notable features include enhanced warming over West Africa and the Sahara (0.27–0.34°C decade^{-1}), strong observed wetting in southeastern Africa (3.99 mm decade^{-1}), and pronounced drying over Madagascar (−6.59 mm decade^{-1})

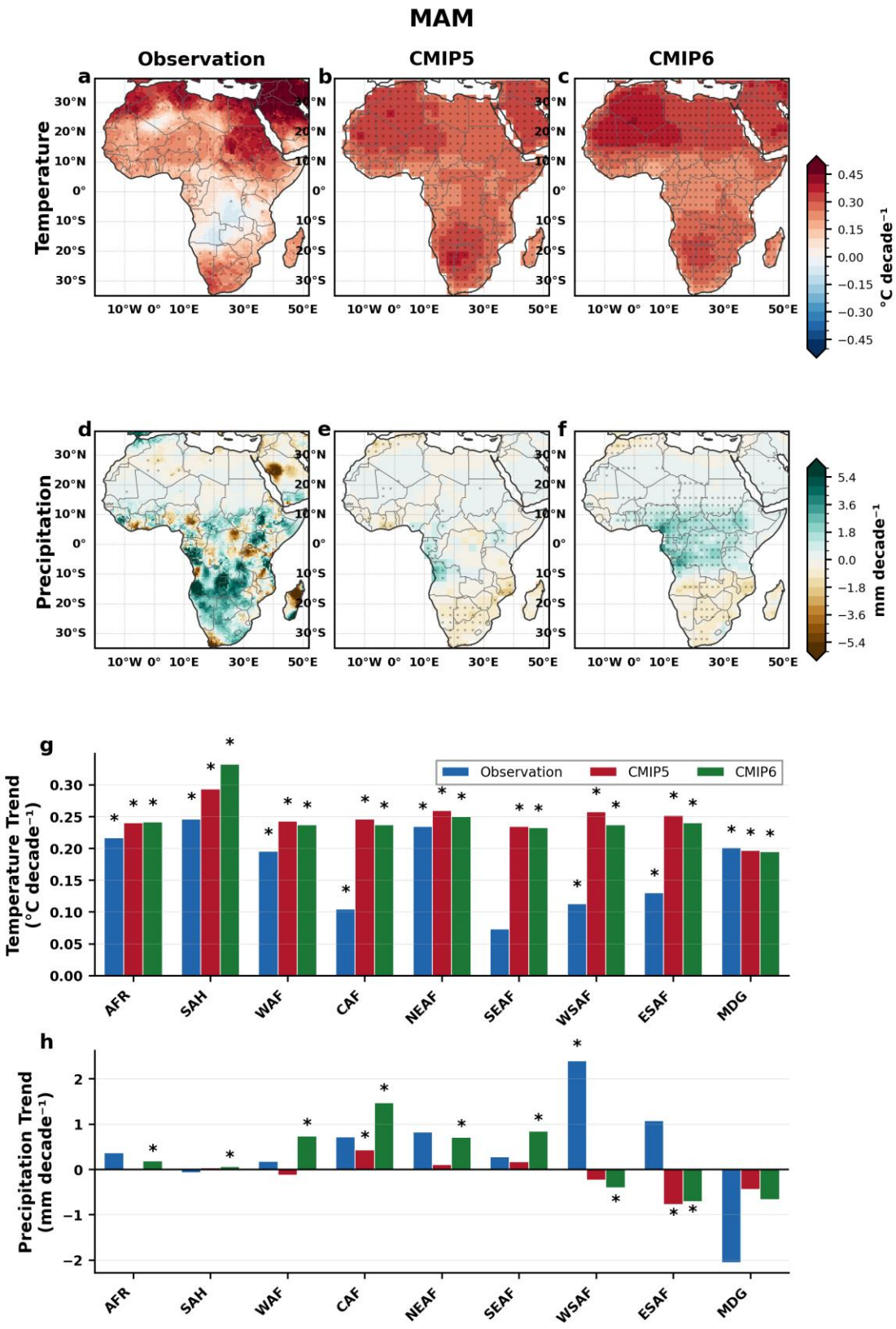

Figure S2: Seasonal temperature and precipitation trends for MAM (March–April–May), 1980–2020. Layout as in Fig. 1. MAM represents the boreal spring transition season. Southeast Africa shows the weakest observed warming (0.07°C decade^{-1}, not significant), while western southern Africa exhibits significant observed wetting (2.40 mm decade^{-1}) that contrasts with model-simulated drying.

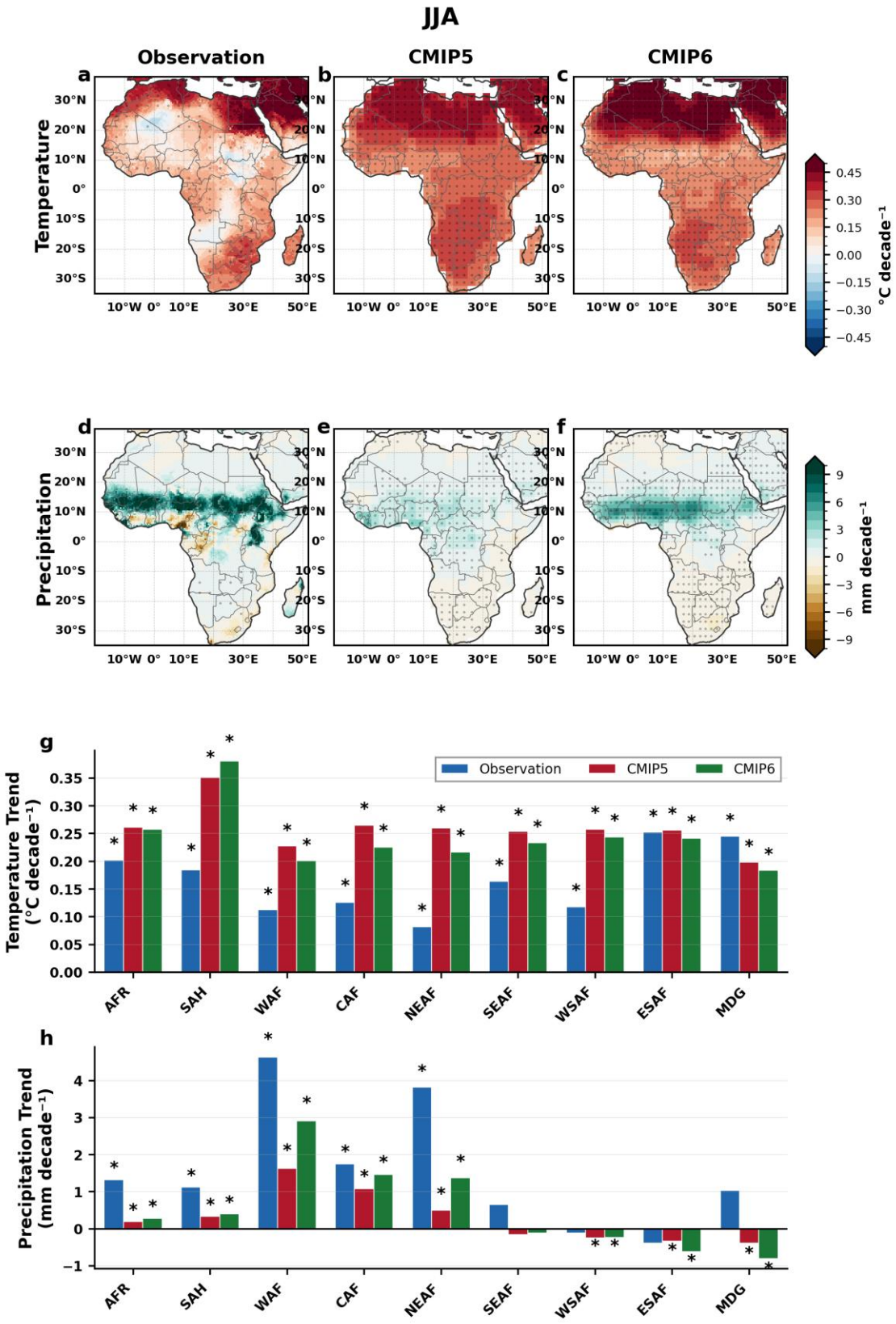

Figure S3: Seasonal temperature and precipitation trends for JJA (June–July–August), 1980–2020. Layout as in Fig. 1. JJA represents the West African monsoon season. Observed precipitation trends peak in West Africa (4.63 mm decade^{-1}) and Northeast Africa (3.82 mmdecade^{-1}), while the Sahara exhibits maximum warming in models (0.35–0.38°C decade^{-1}).

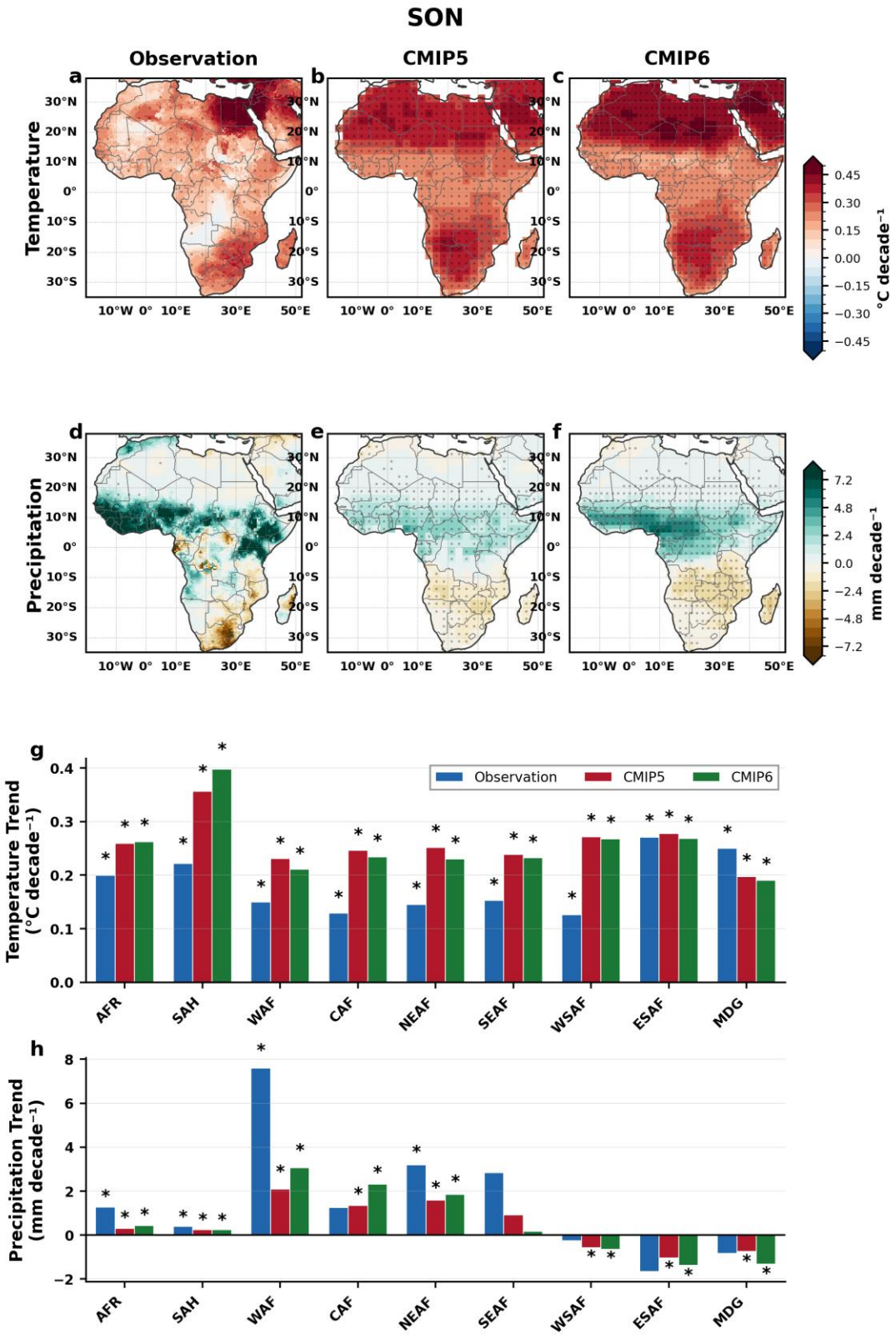

Figure S4: Seasonal temperature and precipitation trends for SON (September–October–November), 1980–2020. Layout as in Fig. 1. SON represents the late monsoon retreat and short rains season. West Africa shows the strongest observed precipitation trends of any season (7.60 mm decade⁻¹), while the Sahara exhibits maximum modelled warming (0.36–0.40°C decade⁻¹). Southern African drying signals are most coherent during this season.

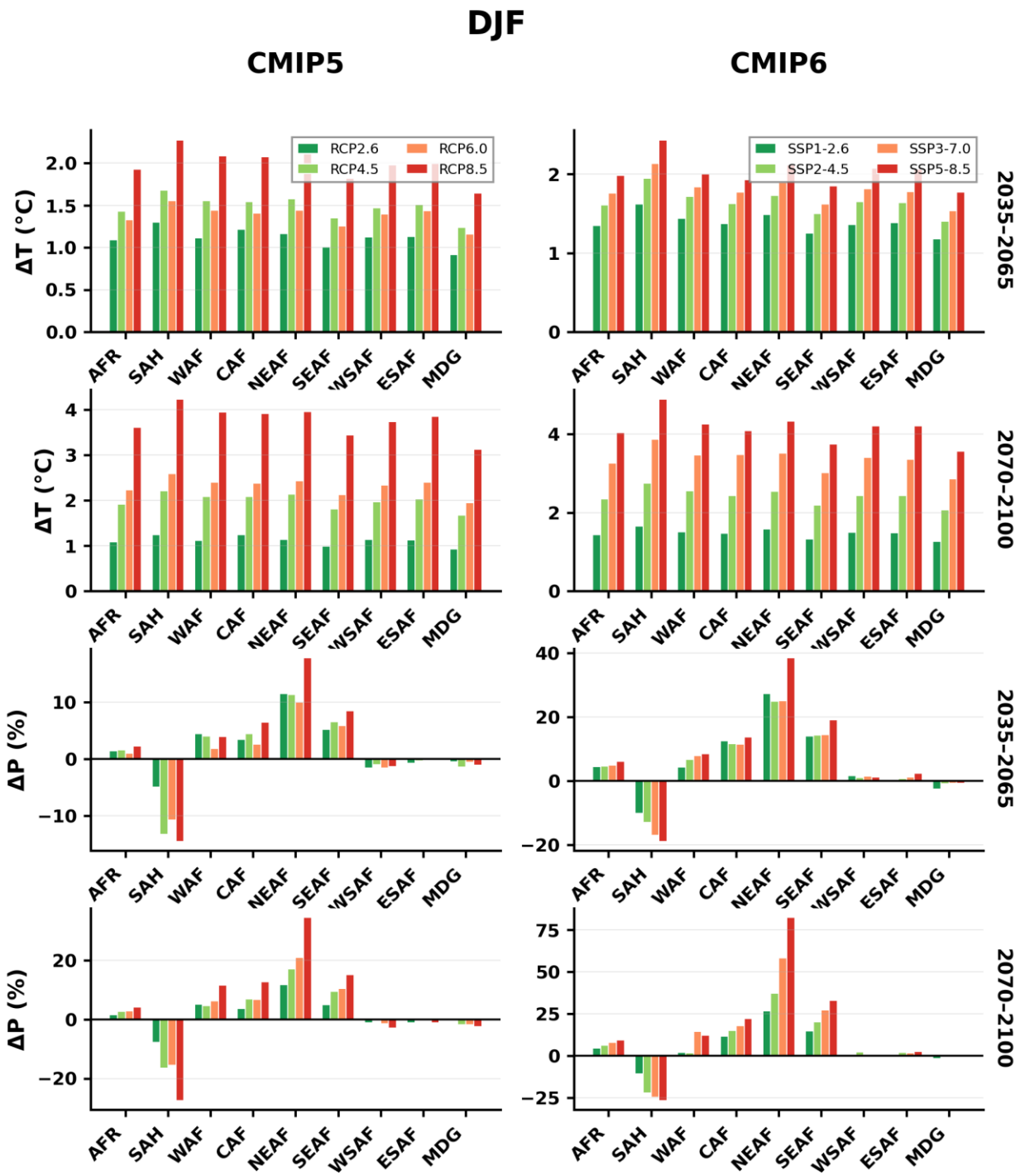

Figure S5: Projected regional mean temperature and precipitation changes across African IPCC reference regions under CMIP5 and CMIP6 emission scenarios for the DJF season. Layout as in Figure 2.

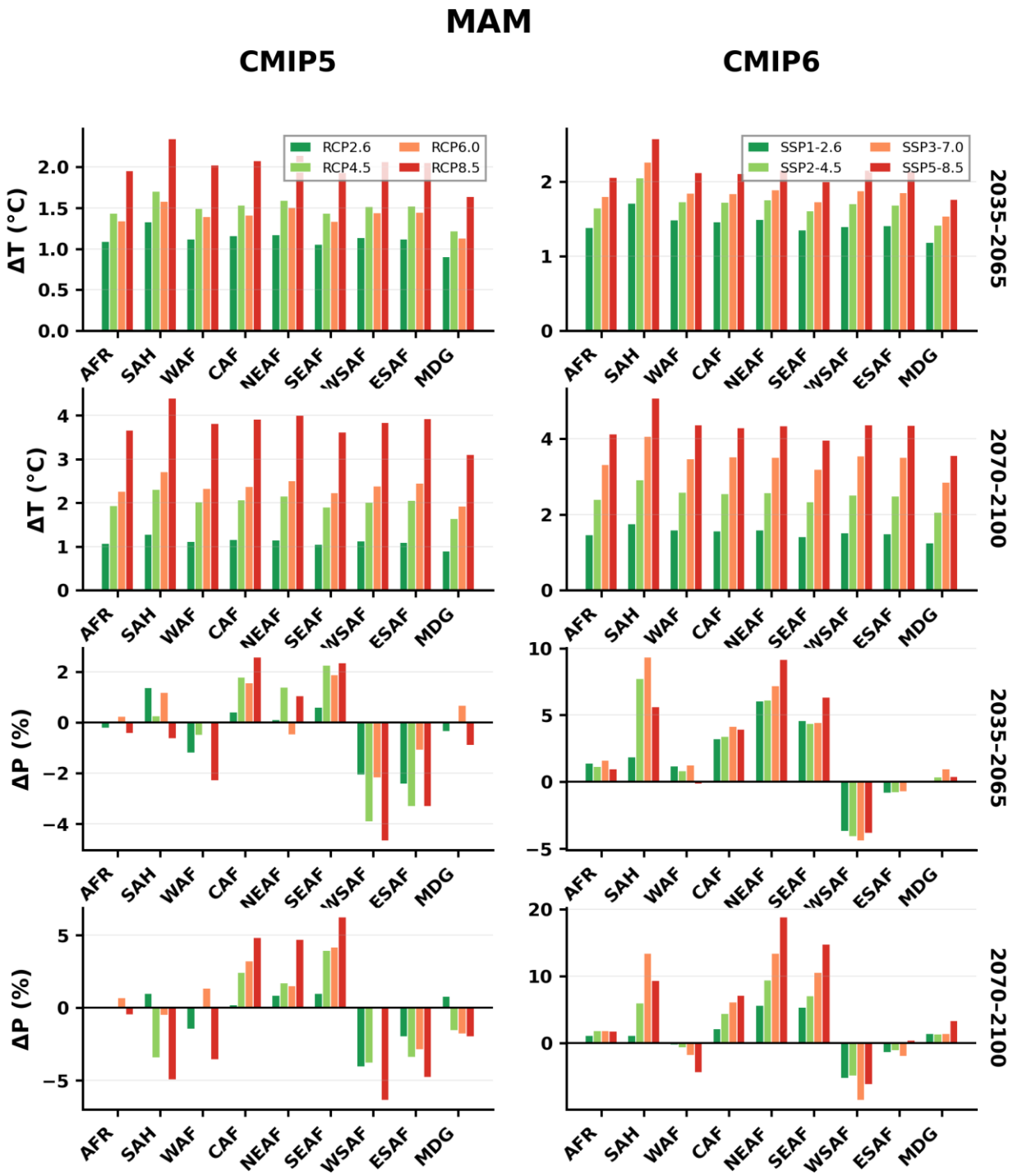

Figure S6: Projected regional mean temperature and precipitation changes across African IPCC reference regions under CMIP5 and CMIP6 emission scenarios for the MAM season. Layout as in Figure 2.

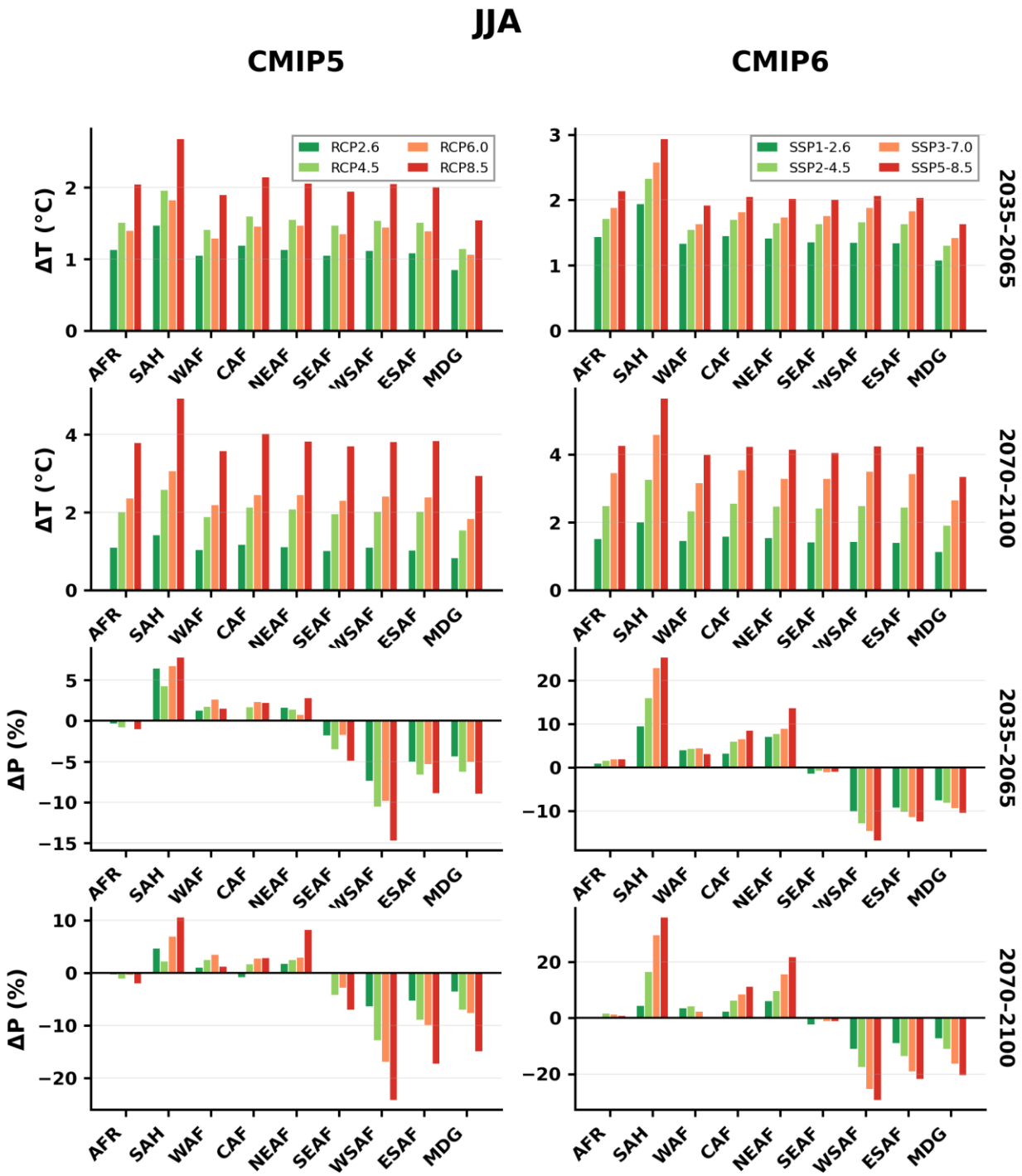

Figure S7: Projected regional mean temperature and precipitation changes across African IPCC reference regions under CMIP5 and CMIP6 emission scenarios for the JJA season. Layout as in Figure 2.

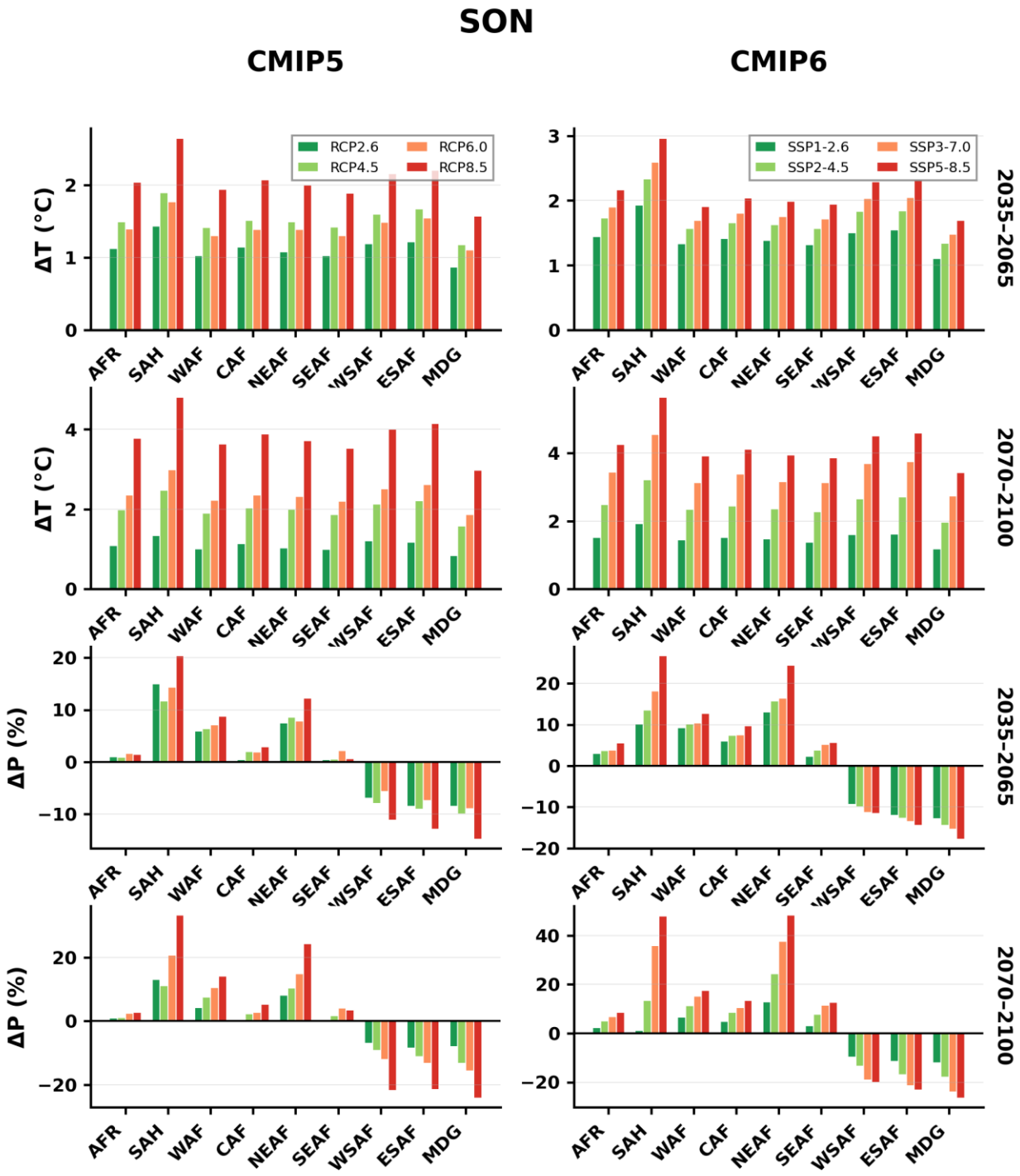

Figure S8: Projected regional mean temperature and precipitation changes across African IPCC reference regions under CMIP5 and CMIP6 emission scenarios for the SON season. Layout as in Figure 2.

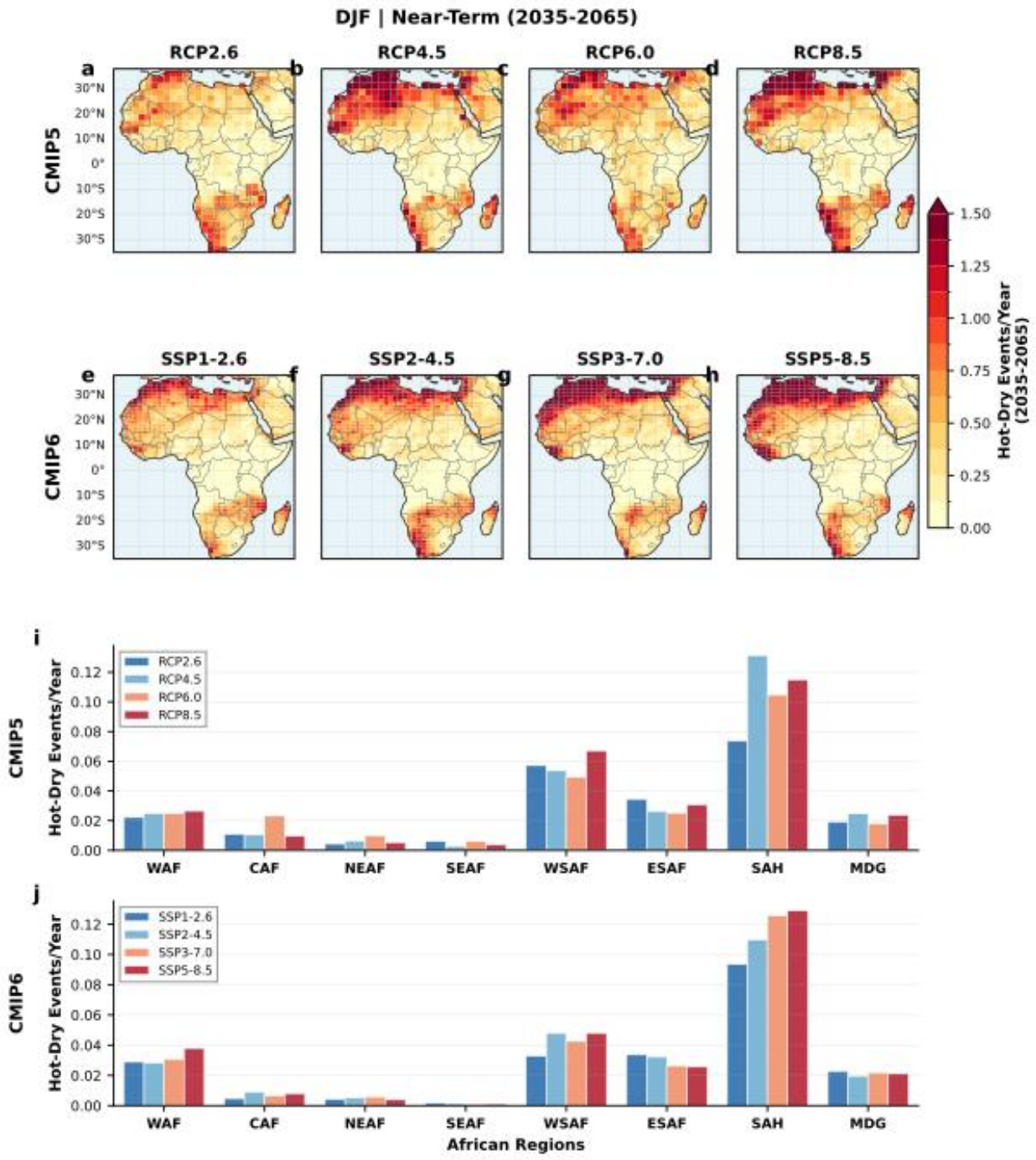

Figure S9: Projected frequency of compound hot-dry extremes across Africa for the near-term period (2035–2065) during the DJF season. Layout as in Figure 3.

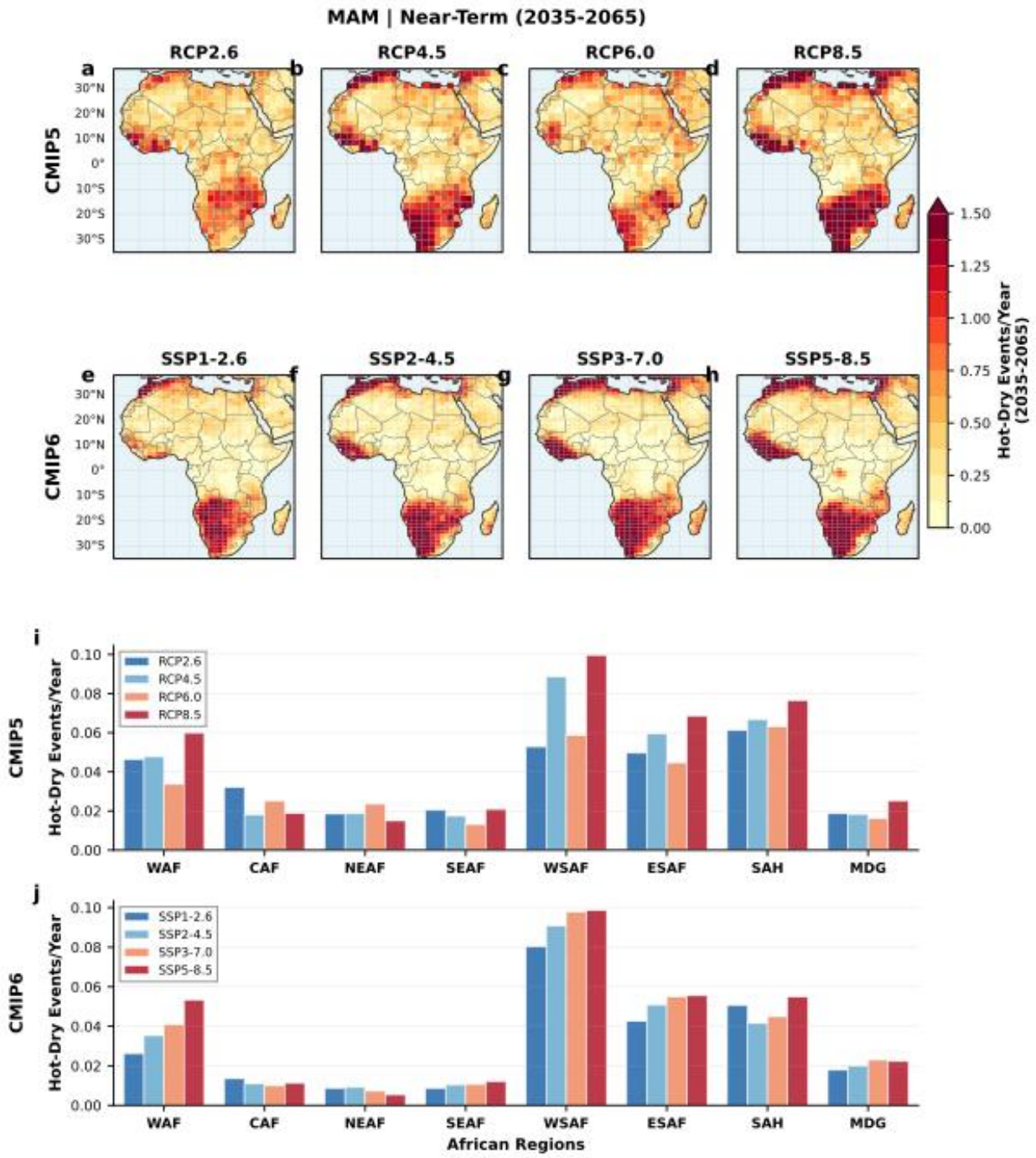

Figure S10: Projected frequency of compound hot-dry extremes across Africa for the near-term period (2035–2065) during the MAM season. Layout as in Figure 3.

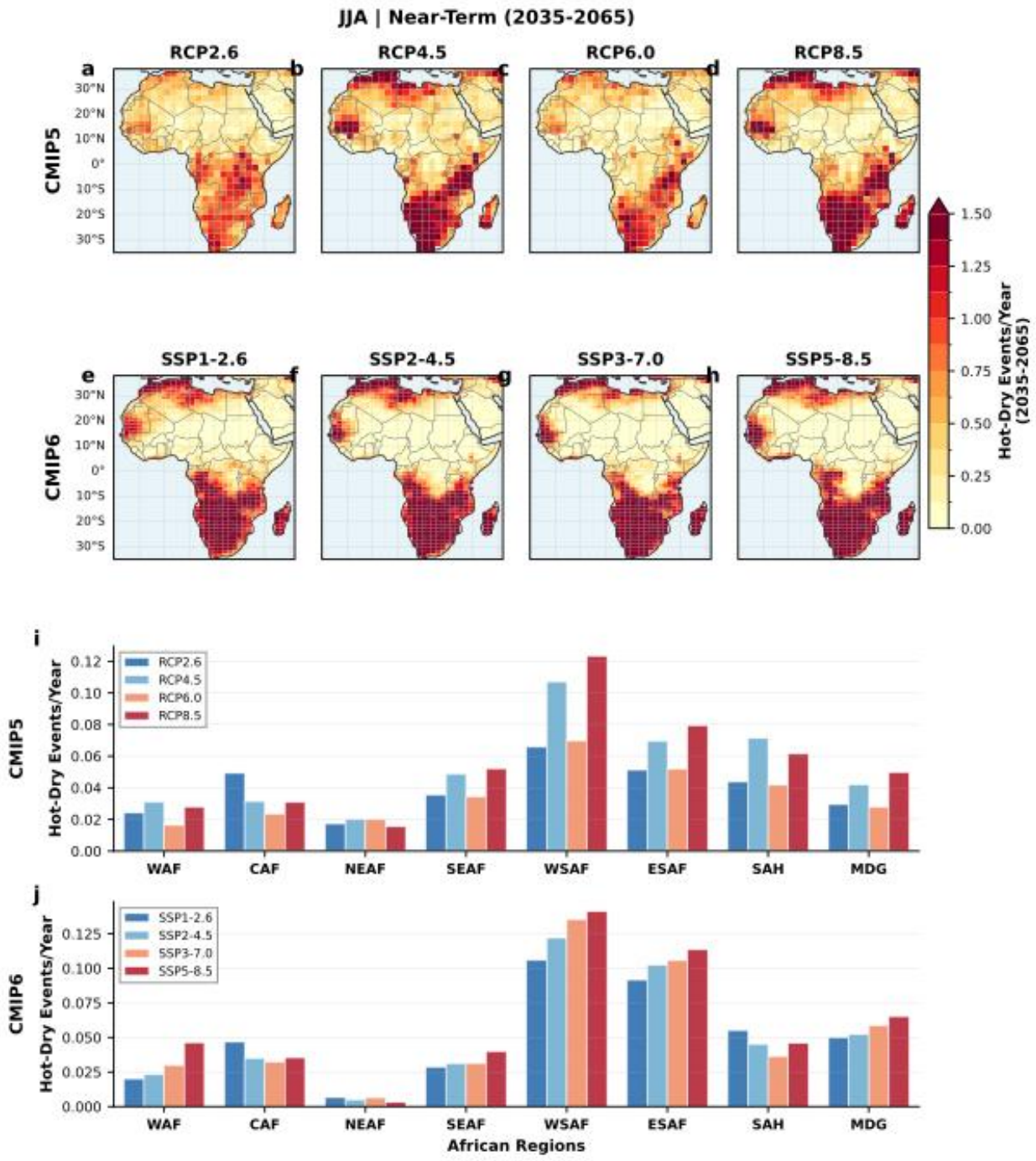

Figure S11: Projected frequency of compound hot-dry extremes across Africa for the near-term period (2035–2065) during the JJA season. Layout as in Figure 3.

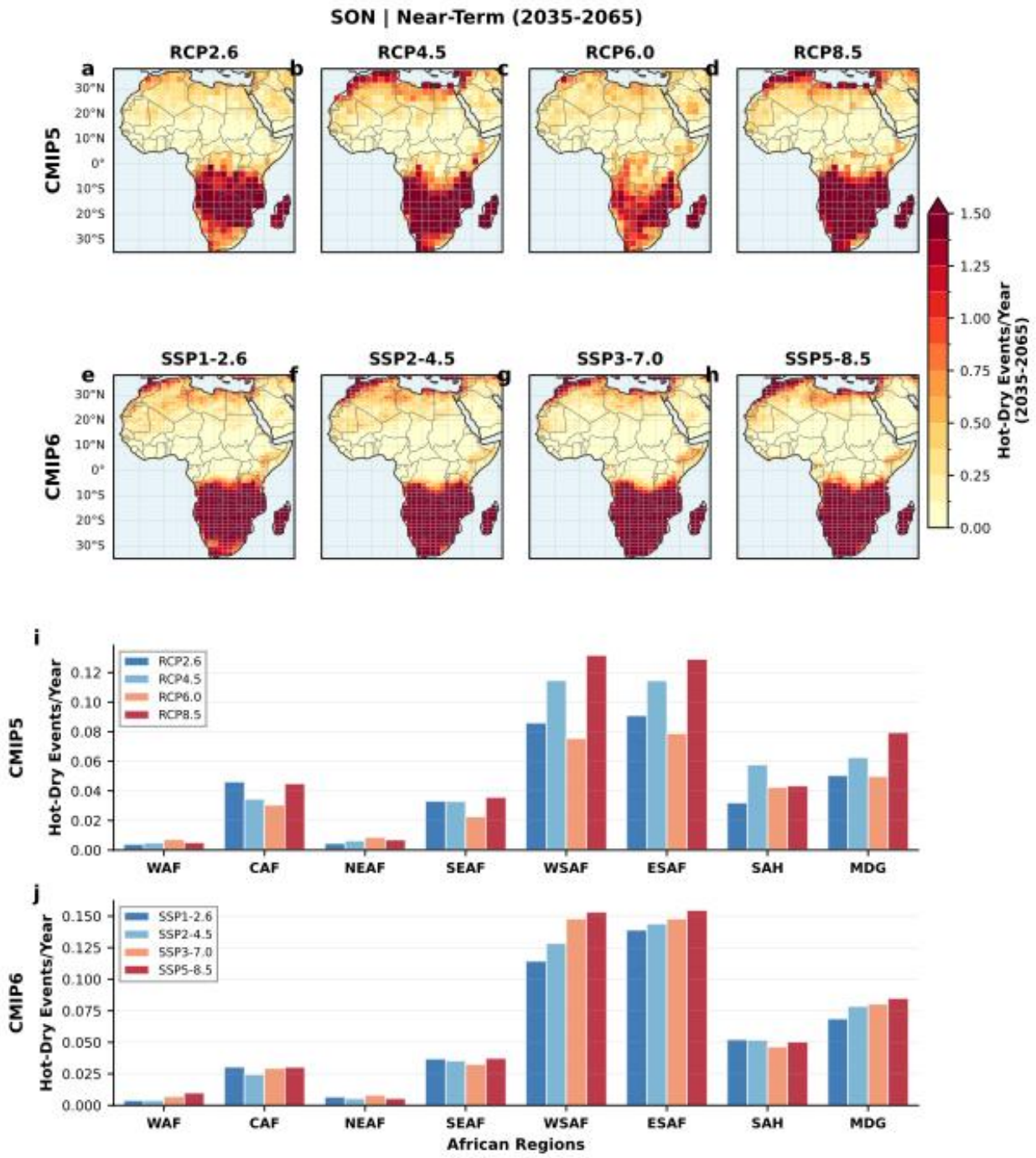

Figure S12: Projected frequency of compound hot-dry extremes across Africa for the near-term period (2035–2065) during the SON season. Layout as in Figure 3.

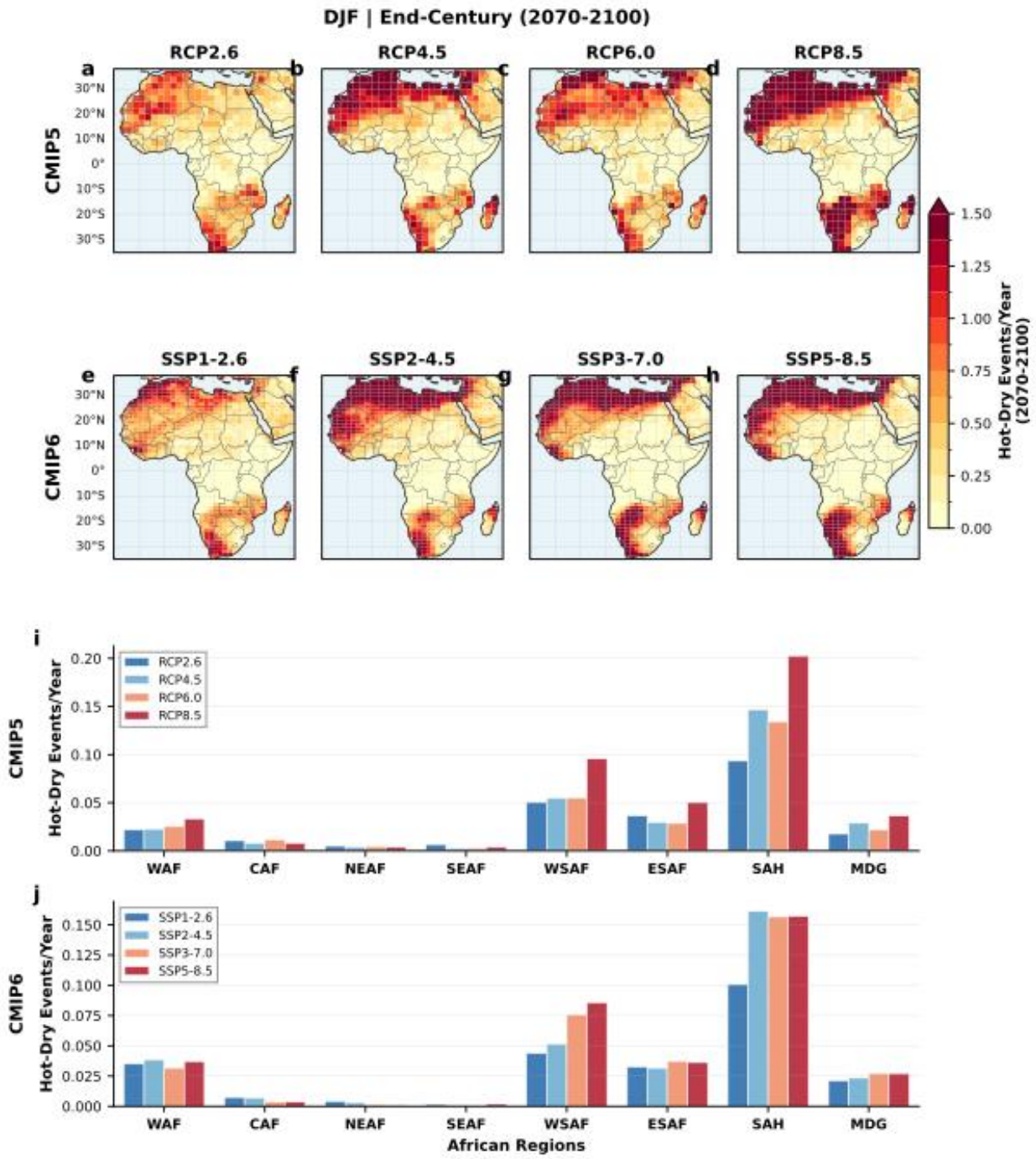

Figure S13: Projected frequency of compound hot-dry extremes across Africa for the near-term period (2070–2100) during the DJF season. Layout as in Figure 4.

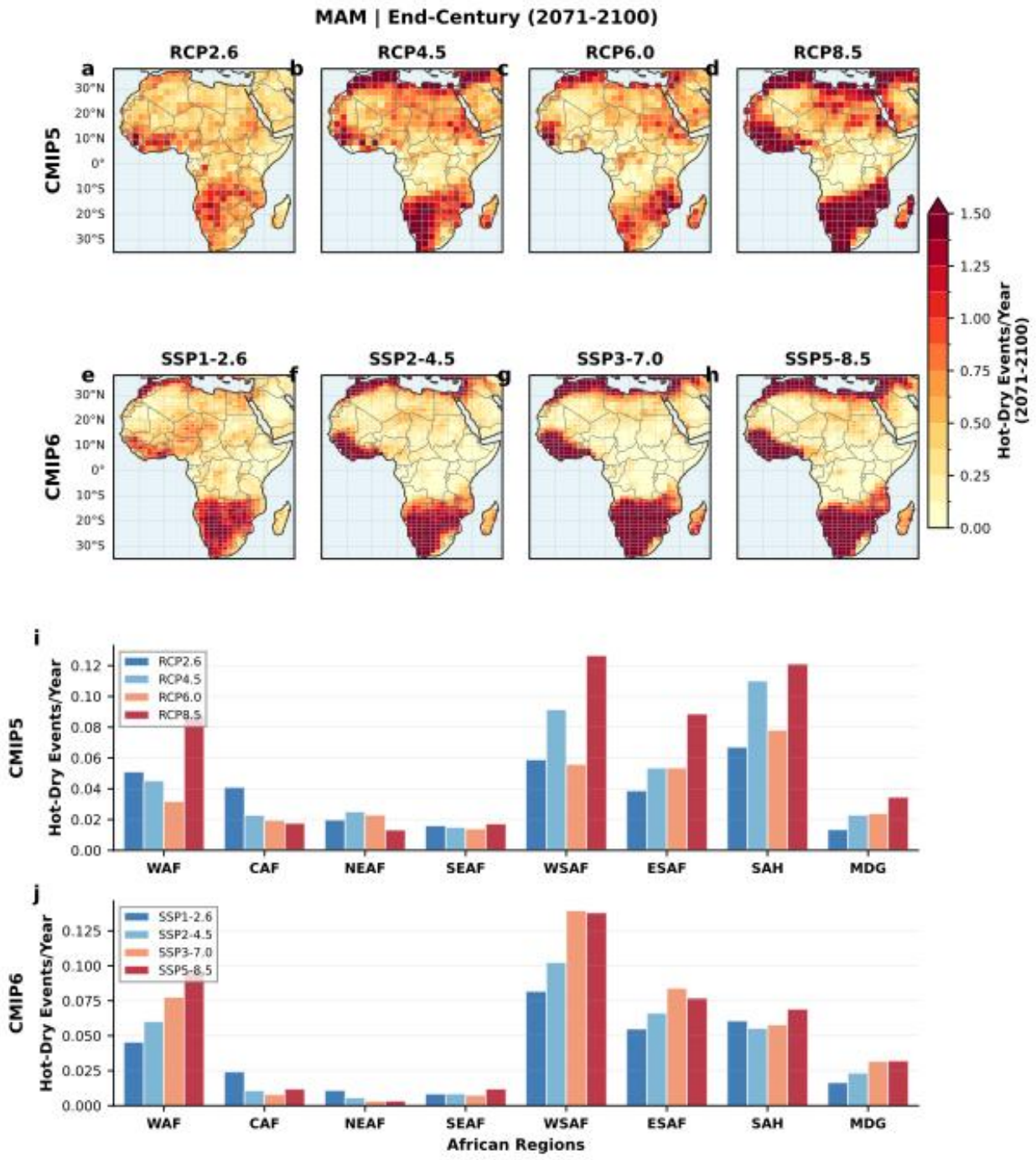

Figure S14: Projected frequency of compound hot-dry extremes across Africa for the near-term period (2070–2100) during the MAM season. Layout as in Figure 4.

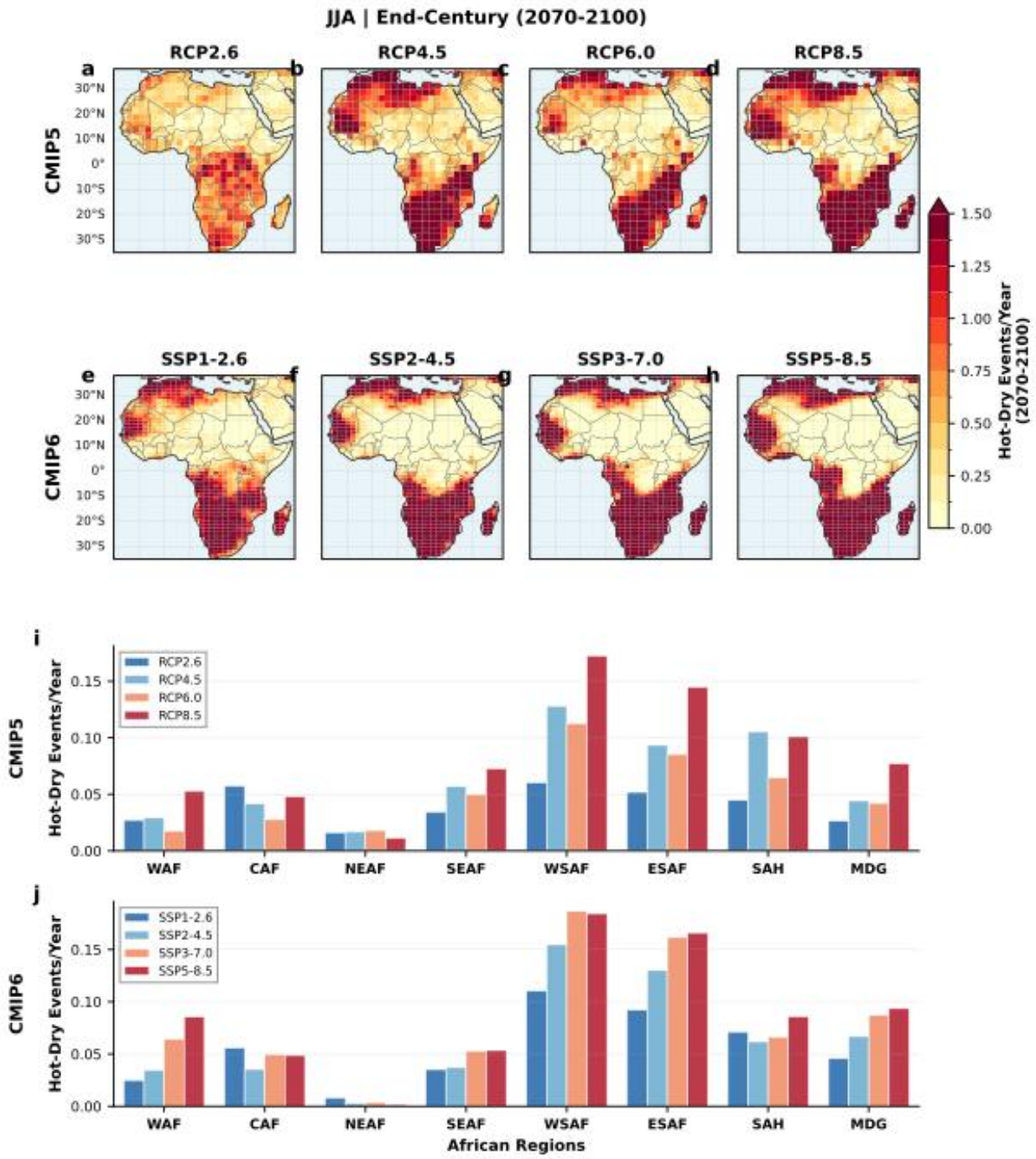

Figure S15: Projected frequency of compound hot-dry extremes across Africa for the near-term period (2070–2100) during the JJA season. Layout as in Figure 4.

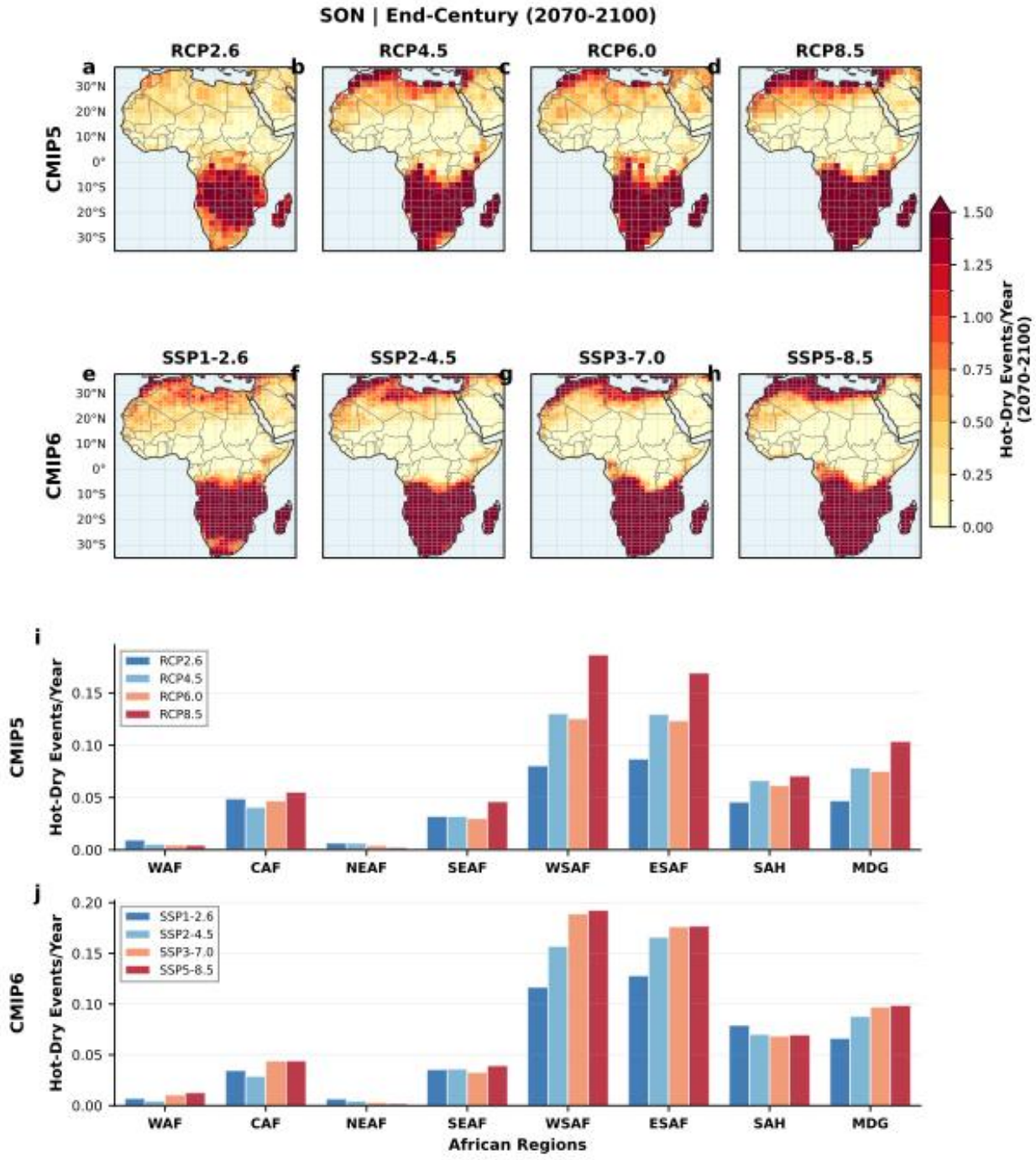

Figure S16: Projected frequency of compound hot-dry extremes across Africa for the near-term period (2070–2100) during the SON season. Layout as in Figure 4.

Table S1: List of CMIP5 Models and Their Developing Institutions/Groups used in the current study

No.	Model Name	Institution/Group
1	ACCESS1-0	CSIRO-BOM, Australia
2	ACCESS1-3	CSIRO-BOM, Australia
3	bcc-csm1-1	BCC, China
4	BNU-ESM	BNU, China
5	CanESM2	CCCma, Canada
6	CCSM4	NCAR, USA
7	CESM1-BGC	NSF-DOE-NCAR, USA
8	CESM1-CAM5	NSF-DOE-NCAR, USA
9	CMCC-CM	CMCC, Italy
10	CMCC-CMS	CMCC, Italy
11	CNRM-CM5	CNRM-CERFACS, France
12	CSIRO-Mk3-6-0	CSIRO-QCCCE, Australia
13	EC-EARTH	EC-EARTH consortium
14	FGOALS-g2	LASG-CESS, China
15	FIO-ESM	FIO, China
16	GFDL-CM3	NOAA GFDL, USA
17	GFDL-ESM2G	NOAA GFDL, USA
18	GFDL-ESM2M	NOAA GFDL, USA
19	GISS-E2-H	NASA GISS, USA
20	GISS-E2-R	NASA GISS, USA
21	HadGEM2-AO	NIMR/KMA, Korea
22	HadGEM2-CC	Met Office Hadley Centre, UK
23	HadGEM2-ES	Met Office Hadley Centre, UK
24	inmcm4	INM, Russia
25	IPSL-CM5A-LR	IPSL, France
26	IPSL-CM5A-MR	IPSL, France
27	IPSL-CM5B-LR	IPSL, France
28	MIROC5	MIROC, Japan
29	MIROC-ESM	MIROC, Japan
30	MIROC-ESM-CHEM	MIROC, Japan
31	MPI-ESM-LR	MPI-M, Germany
32	MPI-ESM-MR	MPI-M, Germany
33	MRI-CGCM3	MRI, Japan
34	NorESM1-M	NCC, Norway
35	NorESM1-ME	NCC, Norway

Table S2: List of CMIP6 Models and Their Developing Institutions/Groups used in the current study

No.	Model Name	Institution/Group
1	ACCESS-CM2	CSIRO-ARCCSS, Australia
2	ACCESS-ESM1-5	CSIRO, Australia
3	AWI-CM-1-1-MR	AWI, Germany
4	BCC-CSM2-MR	BCC, China
5	CESM2	NCAR, USA
6	CESM2-WACCM	NCAR, USA
7	CIESM	THU, China
8	CMCC-CM2-SR5	CMCC, Italy
9	CNRM-CM6-1-f2	CNRM-CERFACS, France
10	CNRM-CM6-1-HR-f2	CNRM-CERFACS, France
11	CNRM-ESM2-1-f2	CNRM-CERFACS, France
12	CanESM5	CCCma, Canada
13	CanESM5-CanOE-p2	CCCma, Canada
14	EC-Earth3	EC-EARTH consortium
15	EC-Earth3-Veg	EC-EARTH consortium
16	FGOALS-f3-L	CAS, China
17	FGOALS-g3	CAS, China
18	GFDL-ESM4	NOAA GFDL, USA
19	GISS-E2-1-G-p3	NASA GISS, USA
20	HadGEM3-GC31-LL-f3	Met Office Hadley Centre, UK
21	INM-CM4-8	INM, Russia
22	INM-CM5-0	INM, Russia
23	IPSL-CM6A-LR	IPSL, France
24	KACE-1-0-G	NIMS-KMA, Korea
25	MIROC6	MIROC, Japan
26	MIROC-ES2L-f2	MIROC, Japan
27	MPI-ESM1-2-HR	MPI-M, Germany
28	MPI-ESM1-2-LR	MPI-M, Germany
29	MRI-ESM2-0	MRI, Japan
30	NESM3	NUIST, China
31	NorESM2-LM	NCC, Norway
32	NorESM2-MM	NCC, Norway
33	UKESM1-0-LL-f2	Met Office Hadley Centre, UK